heritage

MDPI

Article

Digital Facial Approximation of Jebel Irhoud Composite Skull (~315,000 BP)

Cicero Moraes [1], Elena Varotto [2], Michael E. Habicht [2], Francesco Maria Galassi [3,4], Lis Moura [5] and Johari Yap Abdullah [6,7,*]

[1] Ortogonline Treinamento em Desenvolvimento Profissional e Consultoria, Sinop 78557-682, Brazil; cogitas3d@gmail.com
[2] College of Human Sciences and Culture, Flinders University, Adelaide, SA 5001, Australia; elena.varotto@flinders.edu.au (E.V.); michael.habicht@flinders.edu.au (M.E.H.)
[3] Department of Public Health, Experimental and Forensic Medicine, University of Pavia, 27100 Pavia, Italy; francescomaria.galassi@unipv.it
[4] Department of Anthropology, Faculty of Biology and Environmental Protection, University of Lodz, 90-237 Łódź, Poland
[5] Physiotherapist (UNIC) and Zootechnician (UFMT), Sinop 78550-728, Brazil; lisquadros@gmail.com
[6] Craniofacial Imaging Laboratory, School of Dental Sciences, Universiti Sains Malaysia, Health Campus, Kota Bharu 16150, Malaysia
[7] Dental Research Unit, Center for Transdisciplinary Research (CFTR), Saveetha Dental College, Saveetha Institute of Medical and Technical Sciences, Saveetha University, Chennai 602105, India
* Correspondence: johariyap@usm.my

Abstract

The archeological site of Jebel Irhoud, Morocco, houses the oldest fossils attributed to *Homo sapiens*, dated to approximately 315,000 years before present (BP). This study presents a forensic facial approximation based on data from a three-dimensional composite skull derived from Layer 7 of the site, with structural predominance of the Irhoud 1 fossil. The methodology employed open-source software tools, combining anatomical projections and the constrained anatomical deformation technique. Endocast segmentation yielded a volume of 1364 mL, a result fully compatible with measurements and segmentations obtained in previous studies directly from the fossil, while also aligning with the variation observed in modern populations. Two sets of images were produced: an objective approximation in grayscale, focused on osteological correspondence, and a colored artistic version featuring skin pigmentation and facial hair for scientific communication. The results reinforce the feasibility and reproducibility of open-access methodologies applied to paleoanthropology, offering an anatomically coherent representation of this Middle Pleistocene hominin.

Keywords: forensic facial approximation; Jebel Irhoud; *Homo sapiens*; 3D reconstruction; anatomical deformation; paleoanthropology; open-source software

Check for updates

Academic Editor: Arlen F. Chase

Received: 5 August 2026
Revised: 6 September 2026
Accepted: 10 September 2026
Published: 13 September 2026

Copyright: © 2026 by the authors. Licensee MDPI, Basel, Switzerland. This article is an open access article distributed under the terms and conditions of the Creative Commons Attribution (CC BY) license.

1. Introduction

1.1. General Context of the Discoveries

In the early 1960s, during mineral extraction at Jebel Irhoud in Morocco, a worker accidentally uncovered a skull with human-like features. Initial analyses identified it as a fossil of an African Neanderthal variant, dated to approximately 40,000 years before present (BP). Named Irhoud 1, the discovery prompted further excavations that yielded additional fossils and associated stone tools. Over time, improved dating methods revised the age of the finds: in 1991, estimates placed them between 100,000 and 200,000 BP, and in

2007, the date was adjusted to around 160,000 BP [1,2]. Meanwhile, debate grew over the phylogenetic status of fossils, which displayed traits characteristic of both Neanderthals and modern humans [1]. A major shift occurred in 2017, when two articles published in *Nature* reclassified the Jebel Irhoud remains as *Homo sapiens* and proposed a much earlier date of approximately 315,000 BP (±34 ka), making them the oldest known representatives of the species [2,3].

1.2. The Composite Skull

In 2017, the Max Planck Institute for Evolutionary Anthropology (MPI-EVA, Leipzig) publicly released image and video data regarding the three-dimensional digital reconstruction of the Jebel Irhoud skull under a Creative Commons (CC-BY-SA) license [4], as part of the press kit accompanying the publication by Hublin et al. [2] in the journal *Nature*. The three-dimensional model in question constitutes a composite skull, structured through the spatial integration of multiple specimens excavated from the same stratigraphic unit—Layer 7.

Far from being a morphological chimera lacking rigor, the digital alignment yielded a functional and biomechanically coherent anatomical structure obtained via computed tomography [4]. The striking dimension of the mandibular arch and the marked projection of the supraorbital superstructures give the reconstructed assembly a dimensional pattern compatible with an adult individual, exhibiting a robustness consistent with the upper extreme of dimorphic variation observed among the site's specimens [2].

The predominant morphological component of the reconstruction is the Irhoud 1 specimen, the original 1961 discovery. This fossil preserves the neurocranial vault and the upper portion of the viscerocranium—the face and upper alveolar region—of an adult individual, providing the spatial matrix and volumetric orientation for the entire model. The 2017 material even allows for the observation of the cranial vault thickness [4]. The absence of the mandibular element in Irhoud 1 was addressed by incorporating the Irhoud 11 mandible, with teeth present. Meanwhile, the maxillo-alveolar region and upper dental arches were complemented with the assistance of the Irhoud 10 specimen—along with associated dental fragments, such as Irhoud 21 and Irhoud 22 [2,4].

Thus, Irhoud 1 serves as the primary framework of the model, ensuring the anatomical integrity and volumetric orientation of the composite skull, while Irhoud 11, Irhoud 10, Irhoud 21, and Irhoud 22 act as structural completion elements—all originating from the same population, the same archeological layer, and anatomically compatible with one another.

1.3. Scope of the Study

The present study aims to perform the facial approximation of a hominin dated to approximately 315,000 years ago based on the Jebel Irhoud composite skull, employing a combined approach of forensic techniques and anatomical deformation. As a byproduct of the anatomical deformation technique, endocast segmentation is also performed, allowing for volume estimation and subsequent comparison with modern human populations. This study does not intend to evaluate the intrinsic anatomical coherence of the composite skull, but rather to utilize it as a reference geometric framework for the facial approximation.

2. Materials and Methods

2.1. Fundamental Concepts

The foundational data for the facial approximation were extracted from a release accompanied by a press kit provided by the research groups behind the 2017 study [4]. Among the resources supplied by the Max Planck Institute were images and videos licensed under

https://doi.org/10.3390/heritage9090369

Creative Commons (CC-BY-SA), permitting the creation of derivative works provided they are distributed under the same licensing terms. Forensic facial approximation (FFA), also known as forensic facial reconstruction [5], is a recognition-support technique that seeks to reconstruct or estimate facial features from a skull. It is particularly valuable in scenarios where data for individual identification are limited [6]. This study builds on methodologies outlined in [7], beginning with the three-dimensional reconstruction of the skull, followed by the application of anatomical "deformation" techniques [8], refinement of structures based on statistical parameters derived from modern human populations, and finally, detailed finishing of the face, including hair configuration and the production of final images. The virtual donor CT scan originates from an anonymized adult modern human and was acquired with formal written participant consent for digital research purposes. Modeling was performed using *Blender (v.2.91) 3D* software, supported by the *OrtogOnBlender* (v.2.91) add-on (http://www.ciceromoraes.com.br/doc/pt_br/OrtogOnBlender/index.html, accessed on 28 August 2026) and its ForensicOnBlender submodule. Both Blender and the add-on are free, open-source tools compatible with multiple platforms, running on Windows (version 10 or later), macOS (Big Sur or later), and Linux (Ubuntu 20.04 or later). For this work, a desktop computer with the following specifications was used:

- Intel Core i9 9900K 3.6 GHz/16M processor;
- 64 GB RAM;
- GeForce RTX 2070 8 GB GDDR6 256-bit GPU;
- Gigabyte 1151 Z390 motherboard;
- 960 GB SATA III 2.5″ SSD;
- 480 GB SATA III 2.5″ SSD;
- Masterliquid 240 V water cooler;
- Linux 3DCS operating system (https://github.com/cogitas3d/Linux3DCS, accessed on 28 August 2026), based on Ubuntu 20.04.

2.2. Technical Requirements and Workflow

The execution of the workflow described in this study requires prior knowledge of 3D computer graphics (including mesh manipulation, alignment, geometric deformation, and rendering), as well as familiarity with craniofacial anatomy. Accordingly, the proposed approach prioritizes methodological transparency—namely, the explicit description of procedural steps, constraints, and decision points—rather than full automation of the process.

The procedure was conducted in sequential stages, under explicit anatomical constraints. The purpose of this description is to ensure methodological transparency, allowing specialists to understand and critically assess the decisions applied, even though the process involves trained visual judgment by the operator.

Such expert-guided decision points are inherent to forensic facial approximation workflows, particularly when incomplete or composite skeletal material is involved. In these contexts, the operator does not introduce arbitrary morphology, but rather performs constrained adjustments limited by preserved osteological landmarks and structural relationships. The methodological emphasis of the present study is therefore placed on explicit procedural description, anatomical constraints, and reproducibility of the workflow logic, rather than on full automation of the modeling process. This approach allows independent specialists familiar with craniofacial anatomy and 3D modeling to replicate the sequence of operations and critically evaluate the resulting anatomical coherence.

Step 1—Model Preparation (Data Input)

Input: cranial mesh of the target specimen (photogrammetry/specified source), and a virtual donor model (anonymized CT data) used as a geometric reference.

Output: cleaned and standardized models prepared for alignment.

Step 2—Alignment, Scaling, and Orientation

Operations: alignment based on cranial anatomical references; scaling adjustment based on preserved osteological measurements. Minor inter-individual osteological discrepancies among the combined elements (e.g., localized dental mismatches between the incisors and alveolus 21) were deliberately left digitally unadjusted, avoiding manual or biomechanical repositioning to force an artificial dental occlusion.

Fixed constraint: preservation of essential anatomical relationships (e.g., cranial base and orbits), avoiding global distortions not supported by the cranial structure.

Output: models aligned within the same coordinate system.

Step 3—Anatomical Deformation under Constraints

Operations: geometric deformation of the donor model to conform to the morphology of the target cranium.

Fixed constraints: maintenance of fundamental skeletal relationships and overall structural coherence (including endocranial volume and architecture, when applicable).

Operator decision point: fine surface adjustments limited exclusively to compatibility with preserved bony contours, without aesthetic idealization.

Step 4—Soft-Tissue Integration and Controlled Refinement

Operations: application of conservative soft-tissue parameters, with refinements constrained by anatomical coherence.

Fixed constraint: no introduction of volumes or shapes not supported by the cranial structure.

2.3. Forensic Facial Approximation

The initial step was the 3D digitization of the skull, enabled by the photogrammetry tool integrated into OrtogOnBlender (OOB). The video provided in the Max Planck Institute release [4] was obtained and converted into a sequence of images. The resulting mesh was aligned to frontal and lateral views (Figure 1A). Although OOB supports real-scale digitization using ArUco markers, this feature was unavailable in the image sequence, necessitating alternative measures, such as a scale reference included in the aforementioned release (Figure 1B). A tomography of a virtual donor, whose mesh was reconstructed in 3D using OOB tools developed for this purpose, was adjusted to match the morphology of the Jebel Irhoud cranium. This adjustment was performed while preserving geometric coherence between the external craniofacial surface and the internal cranial cavity (Figure 1C), which enabled subsequent segmentation of the endocranium (Figure 1D). The purpose of the anatomical deformation technique is to adapt the donor cranium structure to the target cranium and to propagate this adjustment to the soft tissues, resulting in a facial approximation coherent with the individual's appearance in life. A demonstrative video of the anatomical deformation workflow is provided in the Data Availability Statement section.

As the endocranial cavity can be estimated from the internal surface of the cranium in digital models, and after verifying compatibility between the adjusted donor cranium and the internal slice provided by the team responsible for the original digitization (Figure 1C), the endocranial mesh was extracted (Figure 1D) and its volume measured using the volumetric calculation tools of Blender 3D (https://extensions.blender.org/add-ons/print3d-toolbox/, accessed on 28 August 2026).

To complement the results of anatomical deformation, a nasal projection template was positioned and found compatible with the expected structure (Figure 2A). This template is derived from measurements of soft tissue and bone from computed tomography scans of living individuals of diverse population affinity [8]. The soft-tissue thickness reference values applied in the present study were obtained from datasets representing individuals of African ancestry, as reported by Taylor [9], selected due to their closer geographic and evolutionary relevance to the Jebel Irhoud specimen. In this framework, soft-tissue propagation operates via continuous 3D volumetric mesh deformation conditioned by the underlying osteology, rather than through discrete, point-based soft-tissue depth pegs.

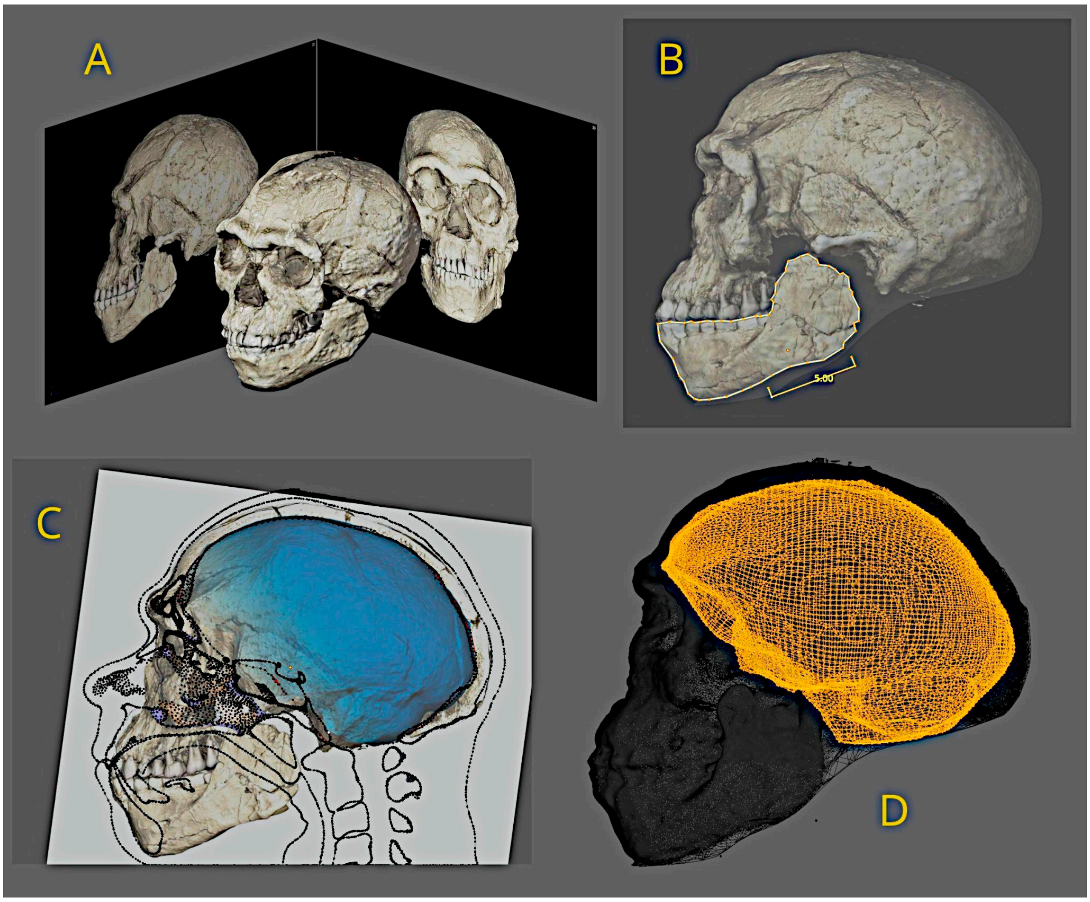

Figure 1. (**A**) Photogrammetry performed from video (credit: Philipp Gunz, MPI EVA Leipzig, License: CC-BY-SA 2.0). (**B**) One of the scale adjustments based on images of the findings. (**C**) Adjustment of the virtual donor to the endocranial structure (credit: Philipp Gunz, MPI EVA Leipzig, License: CC-BY-SA 2.0). (**D**) Segmentation of the endocranium from the anatomical deformation of the virtual donor. References available in [3].

Because no direct soft-tissue data exist for Middle Pleistocene hominins, the use of reference datasets derived from modern human populations represents a necessary methodological proxy rather than an assumption of biological equivalence. The parameters employed in this study were applied under explicit osteological constraints imposed by the fossil morphology, aiming to preserve structural coherence rather than to reproduce a presumed biological profile. Furthermore, variations in soft-tissue depth parameters exert low sensitivity over the global facial geometry, as the deformation process is strictly conditioned and bounded by the underlying cranial morphology. This methodological resilience against modernizing bias was previously demonstrated through comparative interspecies conversions involving highly robust primate osteologies (e.g., between *Gorilla gorilla* and *Pan troglodytes*; see Results and Discussion), confirming that localized tissue thickness adjustments do not override the primary skeletal projections. Consequently, the resulting facial configuration should be interpreted as a morphologically plausible approximation conditioned by the available anatomical evidence, not as a definitive reconstruction of the original individual's appearance or biological characteristics. A video tutorial on this technique is provided in the Data Availability Statement.

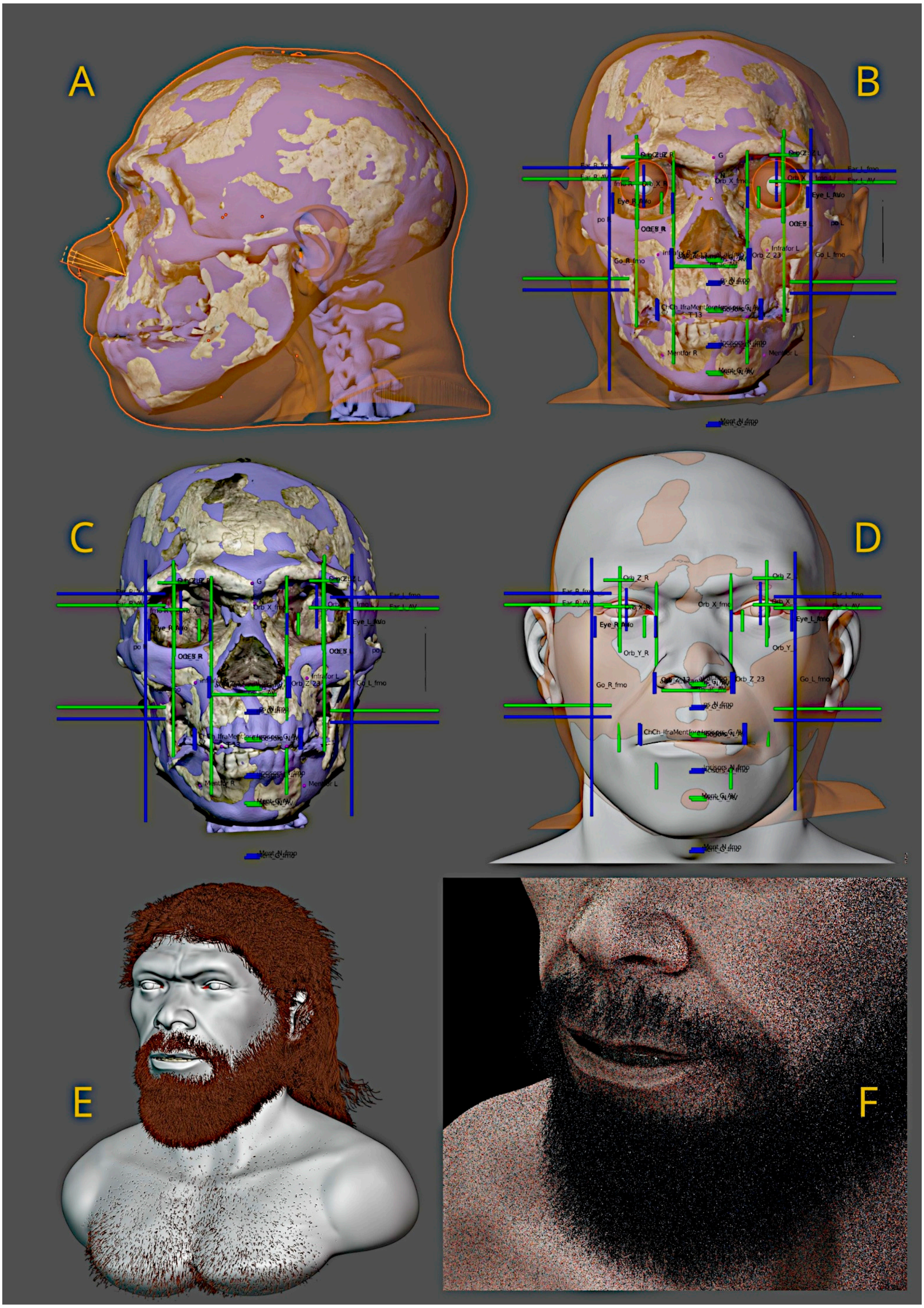

Figure 2. Forensic facial approximation (FFA) process. (**A**) Nasal projection template and anatomical deformation. (**B**,**C**) Projections of the skull and soft tissue elements. (**D**) Basic resulting bust. (**E**) Hair configuration. (**F**) Lighting, color adjustments, and image generation.

The same study addressing nasal profiles was also applied to the frontal projection of the face, covering both soft tissue and the skull (Figure 2B). Examination of the skull revealed significant asymmetry in the right region, corroborated by Holloway et al. [10], with details discussed later. Based on projections using average and proportional structures derived from modern human populations, the Jebel Irhoud skull exhibited a dimension on the X-axis (horizontal) significantly larger than expected for modern reference samples, resulting in a pronounced projection of the lower chin limit on the Z-axis (vertical) [8]. Interestingly, the chin fell between the average (Figure 2C, green line above the chin) and the proportional projection (Figure 2C, blue line below the chin). The gonial angles, however, were smaller than anticipated, as they typically align with the fmo-fmo (frontomalar orbital) points in modern populations. In the analyzed skull, the fmo-fmo distance measured ~118 mm, compared to an average of 96.6 mm (±4.5) [8] in modern populations—approximately 4.75 standard deviations above the expected value. The gonial distance was ~106 mm, compared to an average of 96.9 mm (±6) for modern human populations, representing 1.52 standard deviations above the expected value for the reference sample [8].

To clarify the methodology for projecting facial structures, two video tutorials are available in the Data Availability Statement. In generating the base face, a correction was applied to the midface region (Figure 2D) using soft tissue thickness data from modern individuals [9]. Subsequently, details were digitally sculpted to highlight expression marks, and hair and facial hair were configured (Figure 2E). A demonstration of the particle configuration technique (hair and facial hair) is provided in the Data Availability Statement. The final stage, involving artistic and speculative approaches, included defining skin pigmentation and scene lighting to produce the facial images (Figure 2F). A video exemplifying part of the skin pigmentation process is also provided in the Data Availability Statement.

3. Results and Discussion

3.1. Measurements and Comparisons

The results of this study should be interpreted cautiously, as, although well-documented and supported by extensive references, the analyzed skull is a composite derived from multiple individuals, not representing solely, for example, the Irhoud 1 fossil, but rather an integration of various structures to form a nearly complete specimen. Following a new excavation project initiated in 2004, for instance, the number of identified individuals increased from 6 to 22 [4]. The calvaria appears to correspond to Irhoud 1, the mandible to Irhoud 11, and the upper teeth possibly to Irhoud 10. However, no detailed report on the methodology used in this composition was identified; it is only noted that the mandibular teeth exhibit asymmetry and that the incisor does not align with the alveolus of tooth 21 (upper left incisor). A table listing the 22 identified individuals is available in the supplementary material of Hublin et al. [2].

Several studies on the endocranium of Irhoud 1 have been conducted over recent decades (Table 1), indicating a volume range between 1305 mL and 1480 mL [9,11]. Beyond inherent margins of error, the absence of the lower cranial region may account for this discrepancy, as completing this area allows researchers to make decisions that influence the volume relative to other studies. The present work closely aligns with the findings of [11], which, based on a sample of modern individuals, estimated an average endocast volume of 1328 mL (±164), placing Irhoud 1 within one standard deviation and near this mean. Converting the endocranial volume to brain volume by applying a 9.81% reduction yielded 1230 cm^3, a value very close to the average for modern adult males, which is 1234 cm^3 (±98) [12]. The head circumference, calculated from the reconstructed face, reached 60 cm, placing it 1.58 standard deviations above the adult male average of 56.4 cm (±2.4) [13].

https://doi.org/10.3390/heritage9090369

Table 1. Endocranial volume of Jebel Irhoud 1 (historical data compiled from Holloway et al. [9]).

Author/Study	Volume
Ennouchi (1962) [10]	1480 mL
Anthony (1966) [10]	1480 mL
Holloway (1981) [10]	1305 mL
Neubauer et al. (2018) [11]	1375 mL
Current Study	1364 mL

3.2. Facial Approximation Renderings

Regarding the final facial approximation images, two distinct sets of renderings were produced: (1) a version presented in grayscale and without hair or facial hair (Figure 3); and (2) an artistic variant, comprising colored images that incorporate skin pigmentation, hair configuration, and facial hair (Figure 4). The inclusion of speculative elements in the latter, such as skin tones, lighting, and hair adornments, is not grounded in direct evidence derived from the fossil but reflects artistic conventions informed by anthropological studies of archaic and modern human populations, suggesting plausible traits for an individual from North Africa approximately 315,000 years before the present.

Figure 3. Facial approximation presented in grayscale and without hair or facial hair.

Figure 4. Facial approximation with artistic elements.

Although these subjective features do not accurately represent the individual's appearance in life, the artistic set proves more accessible and appealing to a non-specialist audience, which often demonstrates greater interest and comprehension when presented with visually realistic and humanized depictions. To reduce visual distractions, a facial approximation presented in grayscale and without hair or facial hair was produced (Figure 3), allowing clearer observation of the underlying anatomical configuration in relation to the reconstructed cranium. Thus, the dual approach adopted in this study reconciles the scientific rigor essential to forensic analysis with the didactic and communicative potential of a broader visual presentation, effectively balancing technical precision and educational outreach.

3.3. Complementary Structural Validation

To formally verify the 3D digital scaling and geometric fidelity of the composite model against the primary fossil findings, key craniometric and linear dimensions measured directly on the model were compared with primary published physical data (Table 2). These measurements intentionally prioritized the outermost anatomical boundaries available in the original documentation to validate the macro-spatial scale and overall structural proportionality. The linear values demonstrated strict dimensional correspondence with primary literature sources [2,4], exhibiting only minimal deviations and confirming the accuracy of the photogrammetric spatial reconstruction prior to soft-tissue deformation. Furthermore, the resulting endocranial volume (1364 mL) closely aligns with measurements obtained independently by researchers working directly with CT scan data of the fossil (1375 mL) [11], providing robust secondary cross-validation of the model's volumetric and geometric accuracy.

Table 2. Metric verification comparing key linear dimensions measured on the 3D composite model against published primary literature.

Measure	Our Model (mm)	Source (mm-Reference)
Maximum Skull Length	199.79	201.60 (Max Planck Institute [4])
Bigonial Breadth	152.78	152.37 (Hublin et al. [2])
Length of the Dental Arcade	65.35	66.50 (Hublin et al. [2])
Bi-M3 Breadth	71.16	70.90 (Hublin et al. [2])

In addition to the physical and metric verification against literature sources [2,4,11], it was decided two years after the initial 3D digitization (carried out in 2024)—in 2026, the submission year of this work—to also compare the 3D digitized skull with an independent third-party mesh. For this purpose, an STL file digitized via photogrammetry by Marvin Sevilla and available for download online (https://sketchfab.com/3d-models/jebel-irhoud-1-cranium-reconstruction-d429e3c62c904dd9850d3a79be3438ad, accessed on 28 August 2026) was retrieved. The skull dimensions are fully consistent with the model generated in this work, albeit in his case displaying significantly higher resolution of fine details.

To demonstrate structural compatibility, the simplified STL mesh of the Jebel Irhoud facial approximation bust created in this study was shared and made available for download (https://drive.google.com/file/d/1uyQBh3tLxO7vG9YRyWC9l6hRjRJJSxKs/view?usp=sharing, accessed on 28 August 2026) for direct comparison with Marvin Sevilla's skull and other public models. Visual and spatial examination of the aligned models confirms their structural compatibility (Figure 5), demonstrating consistency with external third-party models created using advanced photogrammetry techniques intended for full-scale 3D printing.

3.4. Empirical Validation, Sensitivity to References, and Methodological Limitations

The anatomical deformation-based facial approximation approach employed in this study was not developed ad hoc for the present case, but rather results from a continuous methodological process that has been applied and tested in different contexts since at least 2013. As detailed in the Section 2 , soft-tissue thickness markers were incorporated as anatomical controls within the deformation process, ensuring consistency with established principles of forensic facial approximation.

Initially, the technique was explored in experimental and exhibition settings, including extreme interspecies tests, such as the deformation of a *Pan troglodytes* craniofacial model into *Gorilla gorilla*, with the aim of evaluating the geometric and anatomical feasibility of the method under morphologically divergent scenarios [14].

These tests demonstrated that, even under substantial variation in reference models, anatomical deformation tends to converge toward morphologically coherent configurations, provided that the structural constraints imposed by the underlying skeletal geometry are respected. This behavior provided the basis for applying the technique to an expanded sample of hominins [15], which was subsequently incorporated into scientific exhibitions on human evolution and is currently part of the permanent collection of the Museo della

Natura e dell'Uomo in Padua (https://visitmnu.it/en/tema/from-the-appearence-of-life-to-homo-sapiens/, accessed on 28 August 2026).

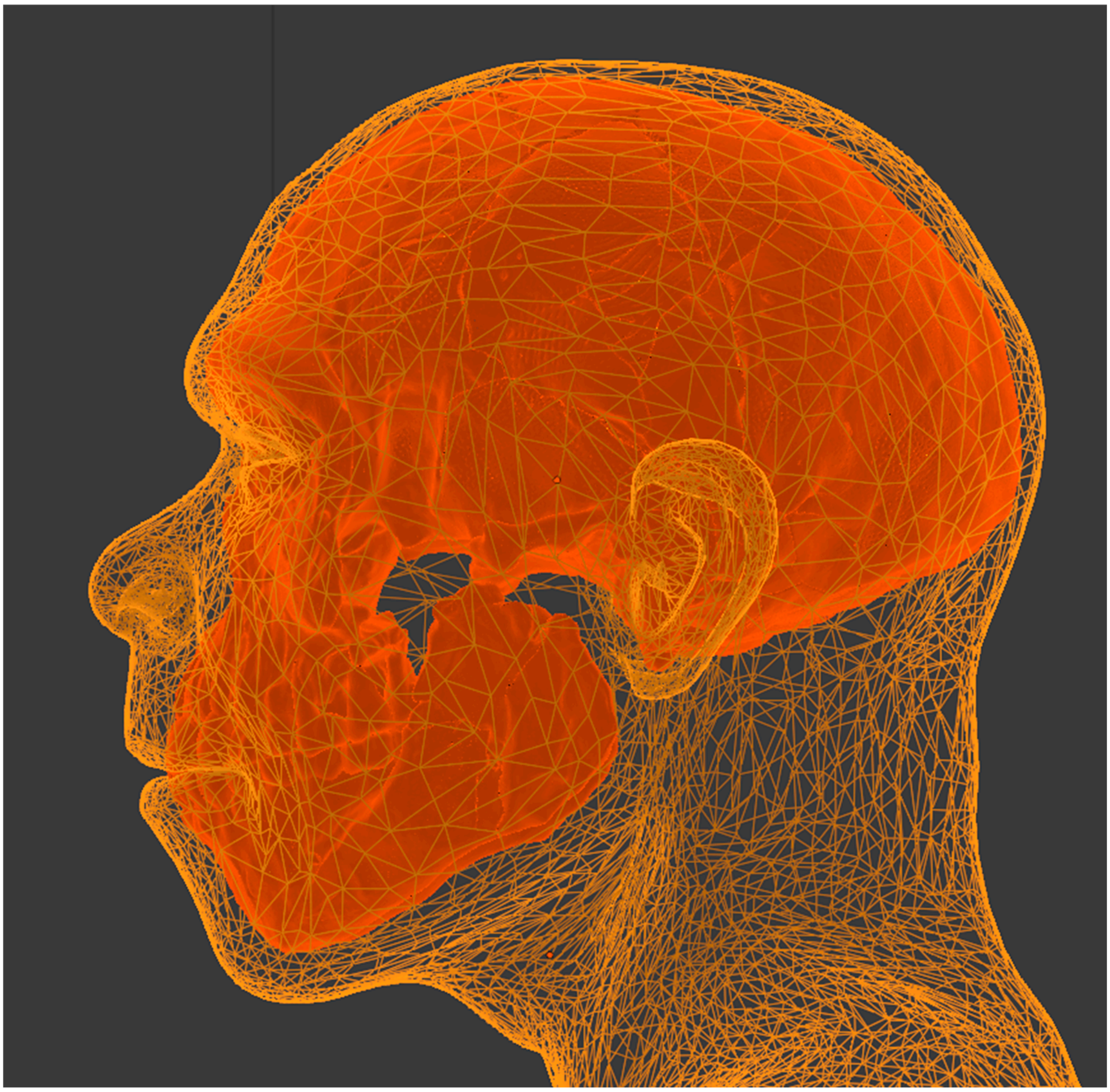

Figure 5. Bust of the facial approximation overlaid on the skull generated by another source. Both are available for download.

The robustness of the approach has also been explored in contexts where direct empirical validation is possible, including facial approximations of historical humans [16] and real forensic cases [17], as well as biomedical and veterinary applications. Examples include published human facial reconstructions, the planning and adjustment of facial prostheses for oncological patients [18], aesthetic planning procedures (such as rhinoplasty) [19], and the fabrication of functional prostheses for living animals based on virtual donor structures adjusted through photogrammetry [20], with subsequent functional verification (https://www.huffpost.com/entry/brazil-tortoise-fire-3d-printed-shell_n_574317f4e4b00e09e89f8416, accessed on 28 August 2026). Regarding the precision of photogrammetry, in addition to the aforementioned applications, this approach has been widely employed in facial surgical planning, demonstrating compatibility with actual anatomy equivalent to that of proprietary and closed-source software [21]. As for anatomical deformation, besides the previously mentioned interspecies conversion case, studies have addressed the conversion of an adult profile into a pre-adolescent one [22] and the adaptation of a model to an individual with achondroplasia from a matrix lacking this genetic condition [23]. Both works were peer-reviewed and published, highlighting the flexibility of the technique and its solid foundation in the scientific literature.

These contexts allowed observation of anatomical convergence between the deformation outcome and the known real morphology, even though the approach does not aim to provide quantitative error metrics.

In the specific case of the Jebel Irhoud specimen, direct validation is not possible, as no preserved soft-tissue reference exists. This limitation is inherent to paleoanthropological material and is explicitly acknowledged in this study. Accordingly, the results should be interpreted as a morphologically plausible approximation, dependent on the adopted references and applied anatomical constraints, rather than as a diagnostic or definitive reconstruction. The primary objective is to demonstrate the internal consistency of the method and its applicability to paleoanthropological contexts within clearly defined limits.

3.5. Study Limitations and Mitigation Proposals

The present study has limitations inherent to both the nature of the analyzed material and the methodology employed, which should be explicitly considered when interpreting the results.

First, the facial approximation necessarily relies on reference data derived from modern human populations, including average soft-tissue thickness parameters and a contemporary virtual anatomical model used as a geometric donor. Although the final outcome retains a subtle relationship with the initial characteristics of the reference model, the anatomical deformation is rigidly guided by explicit osteological constraints, ensuring that the final shape is predominantly dictated by the skull itself. Furthermore, the aforementioned examples of interspecies conversion, differing age groups, and distinct genetic characteristics demonstrate that this approach generates a final model highly consistent with the underlying cranial structure.

Second, the soft-tissue modeling should be interpreted as a morphologically plausible projection rather than a biologically verifiable estimate. No empirical data exist regarding soft-tissue thickness or organization in Middle Pleistocene hominins, and known differences in craniofacial architecture—such as pronounced supraorbital robustness and distinct facial proportions—may have implied muscular and integumentary configurations different from those observed in modern *Homo sapiens*. Consequently, the application of parameters derived from contemporary populations constitutes an interpretative approximation based on anatomical analogy. However, since the final face results from the interpolation of these reference data with the specimen's osteology, anatomical deformation plays a fundamental role in ensuring the structural coherence of the resulting model, harmonizing the estimated thicknesses with the geometric constraints imposed by the skull itself.

Additionally, regarding the endocast volume, although its initial acquisition from a video-digitized model may warrant caution concerning methodological precision, the approach employed demonstrated significant robustness. As presented, the rescaling of the model was strictly anchored in published literature—utilizing linear measurements and calvaria thickness data—resulting in a volume equivalent to that obtained in studies conducted by researchers with direct access to the original fossils. As an additional validation, the methodology was tested against a skull independently digitized by a third party, revealing high geometric compatibility and seamless integration with the proposed facial approximation. Both models have been made publicly available for download to support transparency and reproducibility. Collectively, these indicators demonstrate the coherence, reproducibility, and dimensional accuracy of the adopted approach.

Finally, regarding the composite nature of the skull, as previously noted, the largest and most representative portion of the face derives from a single specimen (Irhoud 1). Regarding the mandible, although belonging to a different individual (Irhoud 10), it corresponds to an adult exhumed from the same archeological stratum and demonstrates remarkable structural compatibility with the cranium, granting the model greater methodological robustness than a reconstruction based solely on theoretical projections. Furthermore, the maxillary dentition, representing a proportionally small region, exerts marginal influence on the final outcome of the facial approximation. It is worth noting that the resulting digital files have been made available for download, allowing interested researchers to conduct their own structural analyses regarding anatomical coherence—a detailed evaluation that transcends the primary scope of the present study.

4. Conclusions

This study demonstrated the feasibility and reproducibility of forensic facial approximation and morphometric analysis of the Jebel Irhoud hominin (~315,000 BP) based on data from a three-dimensional composite skull. By relying exclusively on open-source software tools, the methodology integrated constrained anatomical deformation with projections derived from modern human populations, ensuring that soft-tissue modeling remained strictly bound by the fossil's osteological constraints.

The endocast segmentation yielded a volume of 1364 mL, fully compatible with measurements and segmentations obtained in previous studies directly from the fossil, placing the specimen well within the variation observed in modern human populations. Presenting the results through two complementary approaches—a neutral grayscale version focused on anatomical rigor and a colored artistic depiction—successfully bridges scientific precision with the requirements of public outreach.

Ultimately, these findings reinforce that open-source tools and transparent methodological workflows provide a robust, accessible, and anatomically coherent alternative for the paleoanthropological investigation and reconstruction of complex Middle Pleistocene fossil specimens.

Author Contributions: Conceptualization, C.M. and F.M.G.; methodology, C.M. and J.Y.A.; software, C.M.; validation, F.M.G., L.M., and E.V.; resources, J.Y.A.; data curation, C.M. and M.E.H.; writing—original draft preparation, C.M.; writing—review and editing, F.M.G., J.Y.A., M.E.H., L.M., and E.V.; visualization, C.M. and F.M.G.; project administration, F.M.G. and M.E.H.; funding acquisition, J.Y.A. All authors have read and agreed to the published version of the manuscript.

Funding: This research received no external funding.

Institutional Review Board Statement: Not applicable.

Informed Consent Statement: Not applicable.

Data Availability Statement: The data used in this work are fully available through the links and resources referenced in the article text. Video materials illustrating the practical execution of the workflow and auxiliary procedures are provided as external resources and are listed in this section. These materials are intended solely to complement the manuscript and do not replace the methodological description, which explicitly details the steps, constraints, and decision points adopted in the study. Three-dimensional digitization of faces (and objects) from video: https://ortogonline.com/doc/pt_br/OrtogOnLineMag/2/Video3D.html (accessed on 28 August 2026). Video lecture on the anatomical deformation technique: https://www.youtube.com/watch?v=xig5_EcIFWA (accessed on 28 August 2026). Video lecture on the complementary nasal projection system: https://www.youtube.com/watch?v=F205kLQ--Oo (accessed on 28 August 2026). Facial structure projection: Lesson 1: https://youtu.be/U6oYkEmfyWo (accessed on 28 August 2026). Lesson 2: https://youtu.be/Vcz2e5uSFX8 (accessed on 28 August 2026). Example of hair configuration using particle systems: https://commons.wikimedia.org/wiki/File:D.Pedro_I-_Processo_da_reconstru%C3%A7%C3%A3o_facial_forense.webm (accessed on 28 August 2026). Example of skin pigmentation (texture painting): https://www.youtube.com/watch?v=5lM8PybpKqY (accessed on 28 August 2026).

Acknowledgments: To Bernardo Esteves for his sensitivity in writing an important book on the peopling of the Americas [24], a work that inspired this chapter. To the Max Planck Institute for the media and publications that served as the basis for this material. To Richard Gravalos for providing the computed tomography scan used in this study. A preliminary version of this work was published in Portuguese on the OrtogOnLineMag website (https://ortogonline.com/doc/pt_br/OrtogOnLineMag/9/Irhoud.html, accessed on 28 August 2026) and deposited as a preprint on figshare (DOI: https://doi.org/10.6084/m9.figshare.26038636) on 16 June 2024. That earlier version was not peer-reviewed and has been significantly revised and improved for this submission.

Conflicts of Interest: The authors declare no conflicts of interest. Author Cicero Moraes was employed by the company Ortogonline Treinamento em Desenvolvimento Profissional e Consultoria Ltda. The remaining authors declare that the research was conducted in the absence of any commercial or financial relationships that could be construed as a potential conflict of interest.

References

1. Bruner, E.; Pearson, O. Neurocranial evolution in modern humans: The case of Jebel Irhoud 1. *Anthropol. Sci.* **2013**, *121*, 31–41. [CrossRef]
2. Hublin, J.J.; Ben-Ncer, A.; Bailey, S.E.; Freidline, S.E.; Neubauer, S.; Skinner, M.M.; Bergmann, I.; Le Cabec, A.; Benazzi, S.; Harvati, K.; et al. New fossils from Jebel Irhoud, Morocco and the pan-African origin of Homo sapiens. *Nature* **2017**, *546*, 289–292. [CrossRef] [PubMed]
3. Richter, D.; Grün, R.; Joannes-Boyau, R.; Steele, T.E.; Amani, F.; Rué, M.; Fernandes, P.; Raynal, J.P.; Geraads, D.; Ben-Ncer, A.; et al. The age of the hominin fossils from Jebel Irhoud, Morocco, and the origins of the Middle Stone Age. *Nature* **2017**, *546*, 293–296. [CrossRef] [PubMed]
4. Max Planck Institute. The First of Our Kind—Scientists Discover the Oldest Homo Sapiens Fossils at Jebel Irhoud, Morocco. 2017. Available online: https://www.eva.mpg.de/press/news/2017/2017-06-07-the-first-of-our-kind/ (accessed on 28 August 2026).
5. Stephan, C.N. Facial approximation—From facial reconstruction synonym to face prediction paradigm. *J. Forensic Sci.* **2015**, *60*, 566–571. [CrossRef] [PubMed]
6. Pereira, J.G.D.; Magalhães, L.V.; Costa, P.B.; da Silva, R.H.A. Reconstrução facial forense tridimensional: Técnica manual vs. técnica digital. *Rev. Bras. Odontol. Leg.* **2017**, *4*, 46–54. [CrossRef]
7. Moraes, C.; Suharschi, I. *Mensuração de Dados Faciais Ortográficos em Moldavos e Comparação com Outras Populações*; Figshare: London, UK, 2022. [CrossRef]
8. Quatrehomme, G.; Cotin, S.; Subsol, G.; Delingette, H.; Garidel, Y.; Grévin, G.; Fidrich, M.; Bailet, P.; Ollier, A. A fully three-dimensional method for facial reconstruction based on deformable models. *J. Forensic Sci.* **1997**, *42*, 649–652. [CrossRef]
9. Taylor, K.T. *Forensic Art and Illustration*; CRC Press: Boca Raton, FL, USA, 2000. [CrossRef]
10. Holloway, R.L.; Broadfield, D.C.; Yuan, M.S. *The Human Fossil Record*; Wiley: Hoboken, NJ, USA, 2004. [CrossRef]
11. Neubauer, S.; Hublin, J.-J.; Gunz, P. The evolution of modern human brain shape. *Sci. Adv.* **2018**, *4*, eaao5961. [CrossRef] [PubMed]
12. Ritchie, S.J.; Cox, S.R.; Shen, X.; Lombardo, M.V.; Reus, L.M.; Alloza, C.; Harris, M.A.; Alderson, H.L.; Hunter, S.; Neilson, E.; et al. Sex differences in the adult human brain: Evidence from 5216 UK Biobank participants. *Cereb. Cortex* **2018**, *28*, 2959–2975. [CrossRef] [PubMed]
13. da Costa, N.R.; Mancine, L.; Salvini, R.; Teixeira, J.d.M.; Rodriguez, R.D.; Leite, R.E.P.; Nascimento, C.; Pasqualucci, C.A.; Nitrini, R.; Jacob-Filho, W.; et al. Microcephaly measurement in adults and its association with clinical variables. *Rev. Saúde Pública* **2022**, *56*, 38. [CrossRef] [PubMed]
14. Bezzi, L.; Moraes, C. Archaeological Forensic Facial Reconstruction with FLOSS. Available online: https://www.researchgate.net/publication/281460757_Archaeological_forensic_facial_reconstruction_with_FLOSS (accessed on 13 February 2024).
15. Carrara, N.; Bezzi, L.; Bezzi, A.; Moraes, C. L'approssimazione Facciale Forense: Dallo Studio Alle Mostre Temporanee Fino All'esibizione Permamente [Abstract]. Available online: https://www.musei.unipd.it/sites/musei.unipd.it/files/ANMS%20abstract%20Carrara%20et%20aa.pdf (accessed on 13 February 2024).
16. Moraes, C.; Šindelář, J.; Habicht, M.E.; Sineo, L.; Beaini, T.; Varotto, E.; Galassi, F.M. The Facial Approximation of the Controversial Skull Attributed to Wolfgang Amadeus Mozart (1756–1791). *Anthropol. Rev.* **2024**, *87*, 89–101. [CrossRef]

17. Baldasso, R.P.; Moraes, C.; Gallardo, E.; Stumvoll, M.B.; Crespo, K.C.; Strapasson, R.A.P.; de Oliveira, R.N. 3D Forensic Facial Approximation: Implementation Protocol in a Forensic Activity. *J. Forensic Sci.* **2021**, *66*, 383–388. [CrossRef] [PubMed]
18. Salazar-Gamarra, R.; Cárdenas-Bocanegra, A.; Masch, U.; Da Costa Moraes, C.; Seelaus, R.; Lopes da Silva, J.V.; Lauria Dib, L. Color translation from monoscopic photogrammetry +ID Methodology into a Polyjet final 3D printed facial prosthesis [version 1; peer review: 2 approved]. *F1000Research* **2022**, *11*, 582. [CrossRef] [PubMed]
19. Sobral, D.S.; Duarte, D.W.; Dornelles, R.F.V.; Moraes, C.A.C. 3D Virtual Planning for Rhinoplasty Using a Free Add-On for Open-Source Software. *Aesthetic Surg. J.* **2021**, *41*, NP1024–NP1032. [CrossRef] [PubMed]
20. Rabello, R.; Rabello, M.; Fecchio, S.R.; Moraes, C.; Dias, P.E.M.; Palma, B.; Davanco, R.R. Utilização de Tecnologia 3D Para Reconstituição Protética de Carapaça de Jabuti (*Chelonoidis carbonaria*): Relato de Caso. 2016; *Unpublished*. [CrossRef]
21. Vitorino, N.d.S.; Dias, F.J.d.N.; Daruge, R.J. Photorealistic 3D Facial Meshes Obtained by Low-Cost Photogrammetry: Are They Precise Enough to Replace Colorless CT-scan Meshes in Virtual Surgical Planning? *Braz. Arch. Biol. Technol.* **2026**, *69*, e26250384. [CrossRef]
22. Moraes, C.; Varotto, E.; Artico, M.; Galassi, F.M.; Forte, F.; Habicht, M.E. 3D facial approximation and endocast analysis of the Mummy of Minirdis (Ancient Egypt, ca. 2300 Before Present). *Morphologie* **2024**, *108*, 100781. [CrossRef] [PubMed]
23. Moraes, C.; Krenz-Niedbała, M.; Łukasik, S.; Prada, C.S. Forensic facial approximation of an individual with achondroplasia from medieval cemetery in Central Europe. *Digit. Appl. Archaeol. Cult. Herit.* **2024**, *32*, e00301. [CrossRef]
24. Esteves, B. *Admirável Novo Mundo: Uma História da Ocupação Humana nas Américas*, 1st ed.; Companhia das Letras: São Paulo, Brazil, 2023.

Disclaimer/Publisher's Note: The statements, opinions and data contained in all publications are solely those of the individual author(s) and contributor(s) and not of MDPI and/or the editor(s). MDPI and/or the editor(s) disclaim responsibility for any injury to people or property resulting from any ideas, methods, instructions or products referred to in the content.